

# NJC

Accepted Manuscript



This is an *Accepted Manuscript*, which has been through the Royal Society of Chemistry peer review process and has been accepted for publication.

*Accepted Manuscripts* are published online shortly after acceptance, before technical editing, formatting and proof reading. Using this free service, authors can make their results available to the community, in citable form, before we publish the edited article. We will replace this *Accepted Manuscript* with the edited and formatted *Advance Article* as soon as it is available.

You can find more information about *Accepted Manuscripts* in the [Information for Authors](#).

Please note that technical editing may introduce minor changes to the text and/or graphics, which may alter content. The journal's standard [Terms & Conditions](#) and the [Ethical guidelines](#) still apply. In no event shall the Royal Society of Chemistry be held responsible for any errors or omissions in this *Accepted Manuscript* or any consequences arising from the use of any information it contains.



Journal Name

ARTICLE

## Broadband Photoresponse Promoted by Interfacial Electron Transfer in Diketopyrrolopyrrole-Based Compound/ZnO Hybrid Nanocomposite

Received 00th January 20xx,  
Accepted 00th January 20xx

DOI: 10.1039/x0xx00000x

www.rsc.org/

Hongtao Lin,<sup>a,b</sup> Yishi Wu,<sup>a,\*</sup> Zhenyi Yu<sup>a</sup> and Hongbing Fu<sup>a,\*</sup>

Photoinitiated interfacial electron transfer from organic semiconductor to inorganic one is extremely important in organic/inorganic hybrid optoelectronic materials. Herein, we have prepared hybrid ZnO nanorods by grafting TDPP and TTDPP molecules through carboxyl acid groups, respectively. The steady-state spectroscopic results revealed that the photoluminescence was subjected to severe quenching in the hybrid nanocomposites. Further time-resolved fluorescence and femtosecond transient absorption data verified the occurrence of the interface charge transfer between TDPP or TTDPP molecules and ZnO nanorods in the hybrid nanocomposites. High performance UV-vis photodetectors based on TTDPP/ZnO hybrids have been fabricated and the photoresponsivity of TTDPP/ZnO can approach to 16.9 A/W and on/off ratio as high as 10<sup>4</sup>. The excellent visible-light photoresponse of the hybrid device can be attributed to the broadband absorption after the anchoring of TTDPP compound on the surface of ZnO nanorods, the efficient cascade charge transfer process and the excellent capability of ZnO nanorod to provide direct and stable pathways for the transport of photogenerated electrons toward the collection electrode. This provides guidelines for the construction of organic/inorganic hybrids for optoelectronic application.

### Introduction

Hybrid organic/inorganic nanomaterial has been widely recognized as one of the most promising and rapidly emerging research areas, because it offers high electron mobility or improved spectral coverage for photoconductors, photoswitches and photovoltaic applications.<sup>1-10</sup> In these devices, one photon absorbed by the organic donor material produces a singlet exciton. The generated exciton subsequently diffuses until it reaches the donor-acceptor interface, where it may be dissociated into a pair of charges. That is, photoinduced charge transfer at the organic/inorganic semiconductor interface plays an important role in the performance of these hybrid devices.<sup>11-14</sup> In real devices, the interfacial structures are sophisticated and several reactions take place simultaneously. Hence, the impact of each pathway and the corresponding role in device operation is difficult to distinguish. Inorganic semiconductors have greater electron affinities and higher dielectric constant than the organic materials, so charge transfer at the organic/inorganic interface occurs rapidly. ZnO nanorod is a promising material in organic/inorganic hybrid photoconductor and photovoltaic devices

because of their environmentally friendly, low cost and high electron affinity.<sup>15-18</sup> Recently, Yu et al.<sup>19</sup>, reported an inverted devices using poly thieno[3,4-b]thiophene/benzodithiophene (PTB7):[6,6]-phenyl C71-butyric acid methyl ester (PC<sub>71</sub>BM) as active layer and ZnO as electron transport layer, with a maximum PCE reaching 8.32%. However, until now, hybrid solar cells based on ZnO nanorods and poly-(3-hexylthiophene-2,5-diyl) (P3HT) was lower than 0.6%.<sup>15, 20-23</sup> Friend et al. have developed an "optical pump-push photocurrent probe" technique to study hybrid photovoltaic systems and observed ~50% photogenerated charges stayed in bound charge pair (BCP) states at the organic/inorganic interface and then recombined, whereas, through interface modification with a fullerene derivative decreases the fraction of BCP to ~25%, which substantially improved the device efficiency.<sup>24</sup>

1,4-diketopyrrolo[3,4-c]pyrrole (DPP) compounds are emerging as starting materials for optoelectronic applications.<sup>25-32</sup> It can be easily attached with various electron-rich units via D-A covalent linkage strategy to adjust the HOMO/LUMO energy levels and to obtain low bandgap organic semiconductors.<sup>33-36</sup> For example, Janssen et al.<sup>34</sup>, incorporating biphenyls as co-monomers in electron-deficient diketopyrrolopyrrole (DPP) conjugated polymers enabled widening the optical band gap to 1.70 eV and increasing the power conversion efficiencies to 3.7-5.7% in polymer solar cell. Ashraf et al.<sup>37</sup>, designed a series of diketopyrrolopyrrole-based copolymers with different chalcogenophene comonomers (thiophene, selenophene, and tellurophene) for use in field-effect transistors and organic photovoltaic devices, leading to enhanced field-effect mobilities of 1.6 cm<sup>2</sup>/(V s) and solar cell efficiencies of 7.1-8.8%.

<sup>a</sup>Beijing National Laboratory for Molecular Science (BNLMS), State Key Laboratory for Structural Chemistry of Unstable and Stable Species, CAS Key Laboratory of Photochemistry, Institute of Chemistry, Chinese Academy of Sciences, Beijing P. R. China. E-mail: yswu@iccas.ac.cn; hongbing.fu@iccas.ac.cn

<sup>b</sup>College of Chemical Engineering, Shandong University of Technology, Zibo P. R. China. E-mail: lhtcsh@iccas.ac.cn

† Electronic Supplementary Information (ESI) available: More SEM images and optical measurements. See DOI: 10.1039/x0xx00000x

In order to investigate possible interfacial electron transfer process from DPP derivatives with different HOMO/LUMO energy levels to ZnO and the role of cascade charge transfer on photoresponse properties, we prepared hybrid nanorods by grafting DPP derivatives on the surface of ZnO nanorods using carboxylic acid end group as a functional ligand. Time-resolved fluorescence and femtosecond transient absorption data verified the occurrence of the interface charge transfer between TDPP or TTDPP molecules and ZnO nanorods in the hybrid nanocomposites. High performance UV-vis photodetectors based on TTDPP/ZnO hybrids have been fabricated, which can be attributed to the broadband absorption after the anchoring of TTDPP compound on the surface of ZnO nanorods and the efficient cascade charge transfer process.

## Results and discussion

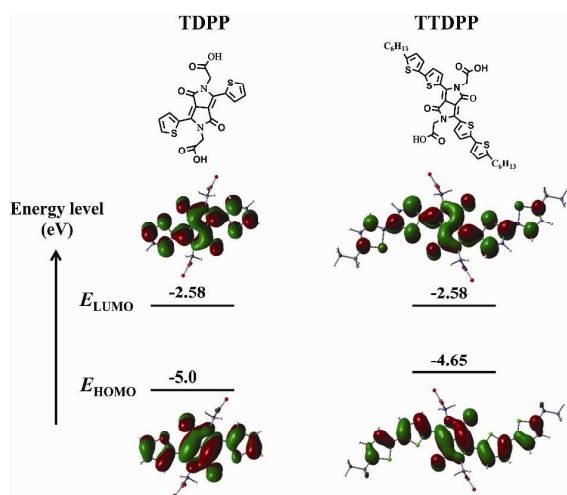


Figure 1. Calculated HOMO and LUMO of TDPP and TTDPP using the DFT method at the B3LYP/6-31G level.

To visualize the electronic structure of TDPP and TTDPP, computational studies were performed by density functional theory at the B3LYP/6-31G level. The HOMO and LUMO of TDPP molecule share similar electron density, which are fully spread over the whole  $\pi$ -conjugated aromatic backbone (Figure 1). In the case of TTDPP molecule, an inhomogeneous electron density distribution is observed. Taking into account the electronic properties of thiophene (electron-rich) and DPP (electron-deficient), the generation of a strongly bound  $\text{T}^{\delta+}$ - $\text{DPP}^{\delta-}$  charge pair may be anticipated. The HOMO level of TDPP and TTDPP locates at -2.58 eV, while the LUMO level of TDPP and TTDPP locates at -5.0 eV and -4.65 eV, respectively.

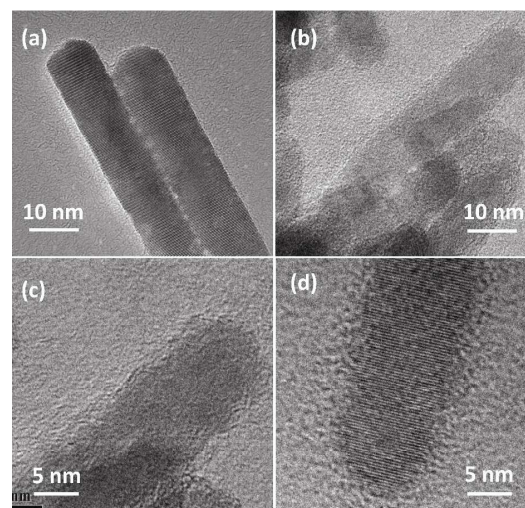


Figure 2. TEM images of the ZnO nanorods (a) before and (b, c) after TDPP, (d) TTDPP compound grafting on the surface of ZnO nanorods.

The as-prepared ZnO nanorods are single crystals with well-controlled sizes of  $12 \pm 4$  nm in diameter and  $100 \pm 15$  nm in length (Figure 2a). TEM images of TDPP/ZnO nanorods show that TDPP surface modification does not alter the nanorod morphology (Figure 2b). HR-TEM analysis of the hybrid TDPP/ZnO and TTDPP/ZnO nanocomposite (Figure 2c and d) indicates that the edge of the hybrid ZnO nanorod become blurred as compared to that of the pure ZnO nanorods, verifying the grafting of organic compound on the surface of ZnO nanorods.

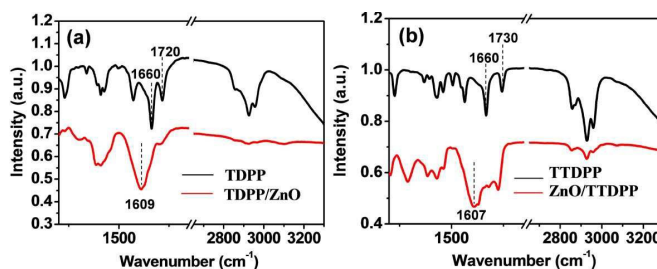


Figure 3. FT-IR spectra of (a) TDPP and (b) TTDPP without and with ZnO attachment.

Figure 3a and 3b show the FT-IR spectra of organic compounds of TDPP and TTDPP and the hybrid composites TDPP/ZnO and TTDPP/ZnO. Figure 3a show the FT-IR spectra of TDPP and TDPP/ZnO solids. The broad  $\text{-OH}$  stretching peak centered at  $2900\text{--}3000$   $\text{cm}^{-1}$  and  $\text{C=O}$  stretching vibration at  $1660$   $\text{cm}^{-1}$  and  $1720$   $\text{cm}^{-1}$  of TDPP solid is factually weak or absent from the spectrum of hybrid TDPP/ZnO. On the other hand, the broad  $\text{O=C=O}$  stretching band at  $1609$   $\text{cm}^{-1}$  in the spectrum of TDPP/ZnO hybrid indicates the formation of carboxylate species with the O atom bonding to single or two neighboring Zn atoms. Similar results were obtained in TTDPP systems (shown in Figure 3b).

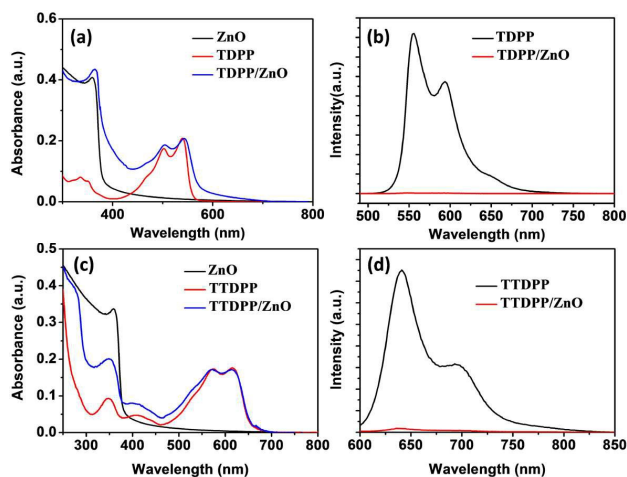


Figure 4. UV-vis absorption spectra of (a) ZnO nanorods, TDPP ( $2.79 \times 10^{-5}$  M in THF), TDPP/ZnO (ca. 2 mg ZnO added to  $2.79 \times 10^{-5}$  M TDPP in THF); (c) TTDPP ( $1.64 \times 10^{-5}$  M in THF), TTDPP/ZnO (ca. 2 mg ZnO added to  $1.64 \times 10^{-5}$  M TTDPP in THF). Fluorescence spectra of (b) TDPP and TDPP/ZnO in THF; (d) TTDPP and TTDPP/ZnO in THF are also shown.

The steady-state spectroscopic measurements show that the absorption spectra are the superposition of features of individual component chromophores, i.e., TDPP, TTDPP and ZnO, respectively (Figure 4a, c). The absorption peak at 365 nm in the UV-vis absorption spectra is ascribed to ZnO nanorods, while the absorption bands in the visible region are due to the organic components. Moreover, the maximum of absorption bands ascribed to the  $S_0 \rightarrow S_1$  electronic transition of TTDPP (620 nm) undergoes a bathochromic shift compared to that of TDPP (525 nm). Accordingly, the optical bandgaps of TDPP and TTDPP reduced from 2.22 eV to 2.00 eV. There is no evidence of any additional absorption peaks in the spectral range measured (250–800 nm), indicating no ground-state charge transfer in TDPP/ZnO and TTDPP/ZnO hybrid nanocomposites. Figure 4b display the fluorescence emission spectra of the compound TDPP and TDPP/ZnO in THF upon excitation at 480 nm. TDPP compound shows a characteristic emission band at 550 nm. The fluorescence quantum yield is  $0.78 \pm 0.05$ . In the case of TTDPP, as shown in Figure 4d, the maximum emission has red-shifted to 640 nm and the fluorescence quantum yield of TTDPP has dropped to  $0.36 \pm 0.02$ . From the above analysis, we can speculate the generation of a strongly bound  $TTDP^{\delta+}$ - $DPP^{\delta-}$  charge pair in TTDPP molecule. However, the fluorescence emission of TDPP/ZnO and TTDPP/ZnO hybrid composites are quenched almost completely, indicative of the interface charge transfer between the organic compounds and ZnO nanorods.

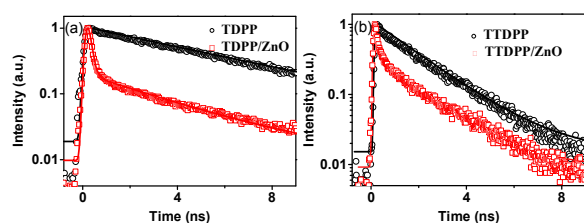


Figure 5. Time-resolved fluorescence spectra of (a) TDPP and TDPP/ZnO in THF solution; (b) TTDPP and TTDPP/ZnO in THF solution.

Time-resolved fluorescence spectra of TDPP and TTDPP were carried out by a streak camera system. It was shown that the fluorescence time profile of TDPP can be fitted with single-exponential decay with time constant of  $5.45 \pm 0.09$  ns (Figure 5a), consistent with the characteristic fluorescence lifetime of DPP derivatives without energy or electron transfer.<sup>38</sup> The time-resolved fluorescence spectroscopy in the case of TDPP/ZnO clarifies that fluorescence time profiles of TDPP can be well fitted with a bi-exponential function (Figure 5a). The minor slow-decaying component of  $3.57 \pm 0.13$  ns (7%) is assignable to residual components of TDPP chromophores. The lifetime of the short-lived component for TDPP/ZnO was  $0.11 \pm 0.005$  ns (93%), which can be safely assigned to the electron-transfer process from TDPP to ZnO nanorod. The time-resolved fluorescence spectrum of TTDPP upon excitation at 610 nm indicates that the emission kinetics is curve-fitted by a single-exponential function of  $1.78 \pm 0.03$  ns (Figure 5b). However, in the case of TTDPP/ZnO hybrid composite (Figure 5b), the fluorescence monitored at 640 nm is approximately curve-fitted by a biexponential function, with a minor slow decay  $1.68 \pm 0.05$  ns (22%) and a major short decay of  $0.11 \pm 0.01$  ns. The major short lifetime can be safely ascribed to the electron transfer from TTDPP to ZnO nanorods. This photoinduced electron transfer mechanism has been already utilized for the construction of ferrocene-PBI linked ensembles in molecular fluorescence switch system.<sup>39</sup> These differences in the distinct fluorescence dynamics of the pristine TDPP, TTDPP and the hybrid TDPP/ZnO, TTDPP/ZnO unambiguously remind us of the possibility that interfacial electron transfer takes place in the hybrid TDPP/ZnO, TTDPP/ZnO systems, which is further supported by transient absorption spectra (vide infra).

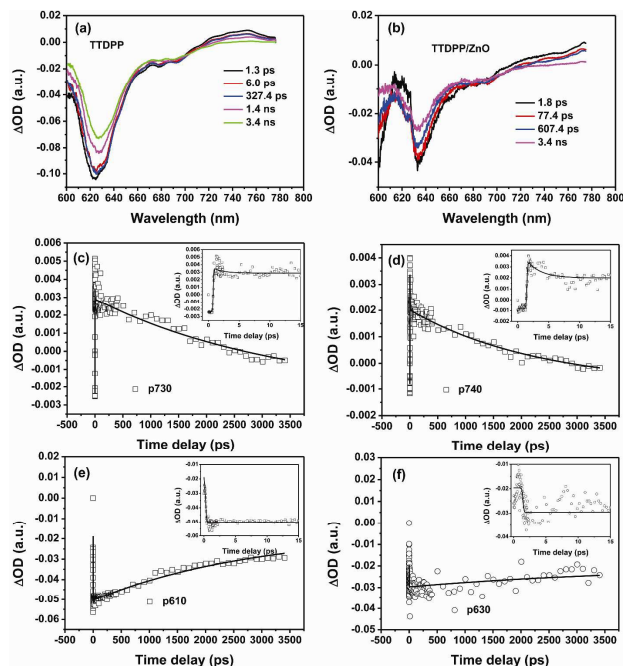
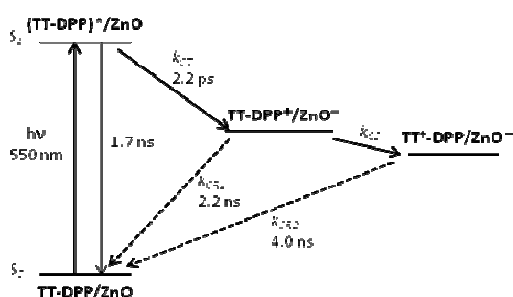


Figure 6. Femtosecond transient absorption spectra of (a) TTDPP and (b) TTDPP/ZnO solution in THF upon excitation at 610 nm with a 130 fs laser pulse with different delay times, as indicated in the spectra. Time-profiles of the transient absorption at (c) 730 nm and (e) 610 nm for TTDPP and those at (d) 740 nm and (f) 630 nm for TTDPP/ZnO. The fit is also shown by the solid lines.

To have a deeper understanding of the photophysics and to further confirm the process of interface electron transfer, TTDPP and TTDPP/ZnO were investigated using femtosecond transient absorption spectroscopy in THF solution. The transient absorption changes were recorded using 130 fs, 620 nm pulses. Figure 6a depicts the transient absorption spectra for TTDPP in THF solution. An intense, broad positive signal covering 700–800 nm is observed. Meanwhile, the negative signal covering 570–700 nm contributes to the ground state bleaching and stimulated emission spectra. Analysis on the 730 nm kinetics results in one slow decaying lifetime of 3.3 ns (Figure 6c). The TTDPP/ZnO hybrid system shows the same spectral patterns as TTDPP (Figure 6b). However, spectral dynamics is obviously shortened. Analysis of the 740 nm kinetics reveals two decaying time constants of 2.2 ps and 2.2 ns, respectively (Figure 6d). The fast component of 2.2 ps can be ascribed to the decay of  $S_1$  state, whereas the slow process is due to the charge recombination of charge transfer (CT) state.

We speculate that interfacial electron transfer resulted in positive polaron on TTDPP and negative polaron on ZnO nanorods. Unfortunately, the polaron state cannot be directly probed within our detecting wavelength range, possibly due to strong superposition with the overwhelming  $S_1$  and/or CT transition state. However, the existence of polaron state can be verified by long-lived ground-state bleaching signal (Figure 6e and 6f). Kinetics analysis of 630 nm traces for TTDPP/ZnO system exhibits a lifetime up to 4.0 ns (Figure 6f), which is much longer than the 2.2 ns decay lifetime derived from the analysis on 740 nm kinetic curve. A new transient species, namely polaron state, produces via interfacial electron transfer between TTDPP and ZnO, is suggested to account for the long-lived ground state bleaching signal.



Scheme 1. Photophysical processes for TTDPP/ZnO hybrid system in THF solution.

Consequently, the detailed photophysical processes in TTDPP/ZnO system can be elucidated and shown in Scheme 1. After excitation, charge transfer from TT to DPP mostly occurred and the transient species  $TT^{\delta+}$ -DPP $\delta^-$  was generated. The charge

recombination depopulates the generated  $TT^{\delta+}$ -DPP $\delta^-$  radical pair. The CT complex mostly underwent interfacial electron transfer from TTDPP to ZnO, promoting the final polaron state. It should be noted that the high dielectric constant of ZnO compared with organic compound promotes efficient decoupling of charge pairs due to the increased screening of the interactions between the positive and negative polaron, suppressing the geminate recombination process in TTDPP/ZnO hybrid systems.

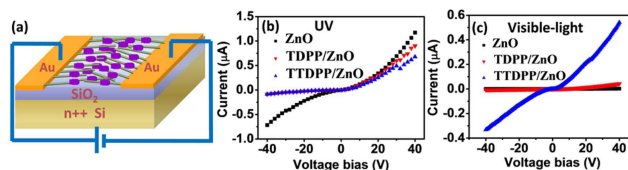


Figure 7. (a) Schematic diagram of the hybrid device. (b)  $I$ - $V$  curves measured under 11.60  $mW/cm^2$  of UV light for ZnO nanorods, TDDPP/ZnO and TTDPP/ZnO nanocomposite. (c)  $I$ - $V$  curves measured under 2.34  $mW/cm^2$  of visible-light for ZnO nanorods, TDDPP/ZnO and TTDPP/ZnO nanocomposite.

We further characterized the photodetector performance of the hybrid nanocomposites. We carried out two-terminal measurements on bulk thin-film samples. Figure 7a is the schematic diagram of the device configuration. The devices were fabricated by drop-casting 5  $\mu L$  of ZnO (20  $mg/\mu L$  in  $CHCl_3$ ), TDDPP/ZnO and TTDPP/ZnO in THF, respectively, on Si/SiO<sub>2</sub> substrate (1  $\times$  2 cm) prepatterned with gold electrodes and drying in air. The thickness of the film is about 150–200 nm estimated by a surface profilometer. The channel width and length are approximately 120 and 5  $\mu m$ , respectively. The scanning electron microscopy (SEM) images of the device shows that the gap is filled with ZnO or hybrid ZnO nanorods, which form a continuous film connecting between Au electrodes (Figure S1). UV light is obtained from a xenon lamp through a band-pass filter (350–360 nm) and the corresponding spectrum is shown in Figure S2a. The visible light is from an iodine-tungsten lamp and the corresponding white-light spectrum is shown in Figure S2b (450–750 nm), which is almost coincident with the absorption of the TTDPP compounds.

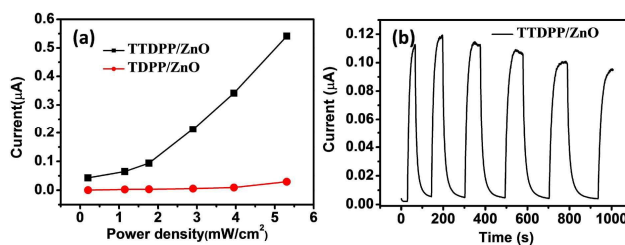


Figure 8. (a) Photocurrents versus light densities of TDDPP/ZnO and TTDPP/ZnO at an electrical field of 8  $V/\mu m$  upon visible illumination. (b) The on/off switching behavior of TTDPP/ZnO device under a visible-light density of 2.34  $mW/cm^2$  and an applied bias voltage of 8  $V/\mu m$ .

ZnO is widely used as an visible-blind UV photodetector. The extremely high UV photoconductive is attributed to the presence of oxygen-related hole-trap states at the surface of ZnO, which prevents charge-carrier recombination and prolongs the photocarrier lifetime.<sup>40,41</sup> As listed in Table 1 and Figure 7b, the UV photo-responsivity ( $R_{ex}$ ) of the device, defined as photocurrent ( $I_{ph} = I_{illum} - I_{dark}$ ) per unit of incident optical power, is 7.4 A/W under 11.60 mW/cm<sup>2</sup> at an electric field of  $E = 8$  V/ $\mu$ m for pure ZnO nanorod film and the on/off ratio is 10<sup>4</sup>. These values are close to that of reported for pure ZnO UV photodetectors in the literatures.<sup>1, 41</sup> Through chemical grafting of TDPP and TTDPP dyes on the surface of ZnO nanorods, the UV-responsivity has slightly changed to 4.6 and 4.3 A/W, respectively, while the on/off ratio to UV light has kept almost unchanged at the same conditions (Table 1). Thus, the anchoring of TDPP and TTDPP compounds on the surface of ZnO nanorods has negligible effects on the UV photodetection property of ZnO, which is attributed to the intrinsically high UV photosensitivity of ZnO.<sup>41, 42</sup>

Table 1. Corresponding responsivity and on/off ratio of ZnO nanorods, TDPP/ZnO and TTDPP/ZnO nanocomposite devices under the illumination of UV and visible-light.

Sample	UV ( $\lambda=355\sim365$ nm)		Visible light ( $\lambda=450\sim750$ m)	
	R(A/W)	On/off ratio	R(A/W)	On/off ratio
ZnO	7.4	$1 \times 10^4$	—	—
TDPP/ZnO	4.6	$2 \times 10^5$	1.35	$3 \times 10^3$
TTDPP/ZnO	4.3	$2 \times 10^5$	16.9	$1 \times 10^4$

ZnO is a poor absorber in the visible region. It can be seen from Figure 7c that the device of pristine ZnO shows almost no visible light photoresponse. Moreover, the device based on TDPP/ZnO hybrid also shows poor visible light photoresponse of 1.35 A/W. In sharp contrast, the hybrid devices of TTDPP/ZnO exhibit excellent visible-light photoresponse characteristics of 16.9 A/W (Table 1 and Figure 7c). For the hybrid devices of TTDPP/ZnO, the dark current ( $I_{dark}$ ) were negligible low around  $7.48 \times 10^{-12}$  A. Upon visible-light illumination with a power density of 2.34 mW/cm<sup>2</sup> at the electric field of  $E = 8$  V/ $\mu$ m, the photocurrent could reach to  $5.41 \times 10^{-7}$  A. The on/off switching ratio for TDPP/ZnO and TTDPP/ZnO devices were about 10<sup>3</sup> and 10<sup>4</sup>, respectively. This is higher than most reported visible-light photodetectors based on ZnO.<sup>16, 43, 44</sup> Additionally, when the light density changed from 0.09 mW/cm<sup>2</sup> to 2.34 mW/cm<sup>2</sup>, the photocurrent of the hybrid TDPP/ZnO and TTDPP/ZnO within the voltage sweep interval increased accordingly (Figure 8a), which could be attributed to more photons absorbed by the photoconductor. In a general case, the photocurrent can be expressed as a power function of the light intensity:  $I \sim P^{C_2}$ , where  $C_2$  corresponds to the photocapture coefficient and determines the response of photocurrent to light intensity.<sup>11, 43, 44</sup> When  $C_2$  tends to 1, all recombination centers are empty, indicating monomolecular recombination in the bulk; when  $C_2$  equal to 0.5, it implies

bimolecular recombination at the surface; When  $C_2$  tends to be a noninteger ( $> 1$ ), it suggests a complex charge carries recombination mechanism through traps or recombination centers in the bulk or on the crystal surface.<sup>45</sup> It can be seen from Table 1 that the visible-light photo-capture coefficient for TTDPP/ZnO hybrids devices is determined to be  $1.3 \pm 0.06$ , indicating an excellent photocapture in the device.<sup>46</sup> The hybrid photodetectors of TTDPP/ZnO showed high stability at the electric field of 8 V/ $\mu$ m and under 2.34 mW/cm<sup>2</sup> visible-light illumination (Figure 8b).

The visible-light photoresponse of TTDPP/ZnO hybrid system is much higher than that of TDPP/ZnO. Taking into account the electronic properties of thiophene (electron-rich) and DPP (electron-deficient), the generation of a strongly bound TT <sup>$\delta^+$</sup> -DPP <sup>$\delta^-$</sup>  charge pair, may be anticipated. The CT complex mostly undergoes interfacial electron transfer from TTDPP to ZnO, promoting the final polaron state or free carrier. Moreover, broad absorption of TTDPP compound as compared with TDPP and the excellent charge transportation property of ZnO nanorods are all contributed to the high visible-light photoresponse of the hybrid TTDPP/ZnO nanocomposite.

## Experimental

### Steady-state spectral measurements

The UV-visible absorption spectra were measured on a Perkin-Elmer Lambda 35 spectrometer with a scanning speed of 240 nm min<sup>-1</sup> and a slit width of 1 nm. Fluorescence emission spectroscopy was performed on a Hitachi F-4500 fluorescence spectrophotometer. The fluorescence quantum yield was determined with a dilute solution ( $A < 0.10$ ) by the comparative method using Rhodamine 6G (FF = 0.95 in C<sub>2</sub>H<sub>5</sub>OH) and cresyl violet perchlorate (FF = 0.54 in C<sub>2</sub>H<sub>5</sub>OH) as standard. The solvents for the measurements were of chromatographic grade and were used as received.

### Quantum chemical calculations

The theoretical calculations were performed with the DFT B3LYP/6-31G method and the GAUSSIAN-03 software package.<sup>51</sup> The optimized configurations and frontier orbitals were generated using the GaussView software.

### Time-resolved fluorescence spectroscopy

Fluorescence kinetics were measured using a picosecond time resolved fluorescence apparatus, which has been described in detail elsewhere.<sup>47</sup> Briefly, the excitation laser pulses (620 nm) were supplied by an optical parametric amplifier (OPA-800CF, Spectra Physics), which was pumped by a regenerative amplifier (Spitfire, Spectra Physics). The excitation pulse energy was  $\sim 100$  nJ pulse<sup>-1</sup> at a pulse repetition rate of 1 kHz, which was focused onto a spot 0.5 mm in diameter. The photoluminescence was collected with a 90 degree geometry, dispersed by a polychromator (250is, Chromex) and collected with a photon-counting type streak camera (C5680,

Hamamatsu Photonics). The data detected by the digital camera (C4742-95, Hamamatsu) were routinely transferred to a PC for analysis with HPDTA software. The spectral resolution was 2 nm and the temporal resolution was 20-100 ps depending on the delay-time range setting. Analysis of the kinetic traces derived from the time-resolved spectra was performed individually using nonlinear least-square fitting to a general sum-of-exponentials function after deconvolution of the instrument response function (IRF). All the spectroscopic measurements were carried out at room temperature unless otherwise stated.

### Femtosecond transient absorption spectroscopy

A Ti:sapphire femtosecond laser system provided laser pulses for the femtosecond transient absorption measurements. A regenerative amplifier (Spitfire, Spectra Physics) seeded with a mode-locked Ti:sapphire laser (Tsunami, Spectra Physics) delivered laser pulses at 800 nm (130 fs, 1 kHz), which were then divided into two components using a 9:1 beam splitter. The major component was sent to an optical parametric amplifier (OPA-800CF, Spectra Physics) to generate the pump pulses (620 nm, 130 fs, 1 kHz). The minor component was further attenuated and focused into a 3 mm sapphire plate to generate the probe pulses. A band-pass filter (SPF-750, CVI) was inserted into the probe beam to a select visible probe (680-790 nm) and a long-pass filter (HWB850, Nantong) for the near-infrared probe (840-1020 nm). The time delay between the pump and probe beams were regulated through a computer-controlled motorized translation stage in the probe beam. A magic-angle scheme was adopted in the pump-probe measurement. The temporal resolution between the pump and the probe pulses was determined to be 150 fs (FWHM). The transmitted light was detected by either a CMOS linear image sensor (S8377-512Q, Hamamatsu) or an InGaAs linear image sensor (G9203-256D, Hamamatsu) when necessary. The excitation pulsed energy was 0.2 mJ pulse<sup>-1</sup> as measured at the rotating solution sample cell (optical path length: 1 mm) or a fixed solid sample holder. A typical absorbance of 0.4 at the excitation wavelength was used. The stability of the solutions was spectrophotometrically checked before and after each experiment.

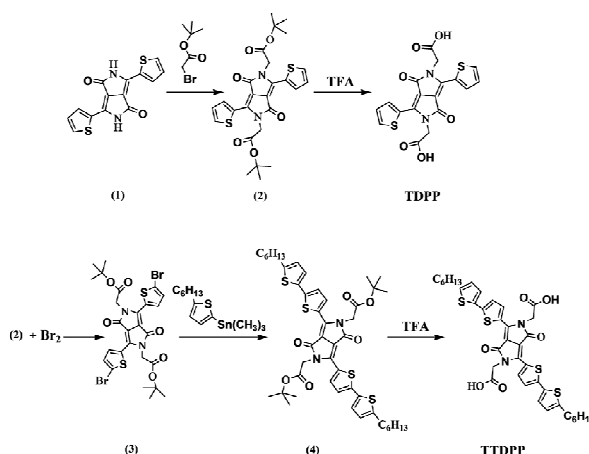
### Characterization of the morphology

The morphology of the nanobelts was imaged by a Hitachi S-4800 scanning electron microscope (SEM), transmission electron microscopy (TEM, JEOL JEM-2011).

### Photodetector device fabrication

The devices were fabricated by drop-casting 5  $\mu\text{L}$  of ZnO (20 mg/ $\mu\text{L}$  in  $\text{CHCl}_3$ ), TDPP/ZnO and TTDPP/ZnO in THF, respectively, on Si/SiO<sub>2</sub> substrate (1  $\times$  2 cm) prepatterned with gold electrodes and drying in air. The thickness of the film is about 150-200 nm estimated by a surface profilometer. The channel width and length are approximately 120 and 5  $\mu\text{m}$ , respectively. All the electrical characterizations were performed in air using a Keithley 4200 instrument under an ambient atmosphere.

### Synthesis of TDPP and TTDPP



Scheme 2. Synthetic Procedures of TDPP and TTDPP molecules.

Compound **(2)**<sup>48</sup>: 3,6-Di(thiophen-2-yl)pyrrolo[3,4-c]pyrrole-1,4(2H,5H)-dione (**1**, 3.5 g, 11.7 mmol) and K<sub>2</sub>CO<sub>3</sub> (4.02 g, 0.029 mmol) was dissolved in anhydrous DMF. Subsequently, tert-Butyl bromoacetate (5.68 g, 0.029 mmol) was added in one portion and the mixture was stirred at 120 °C for 24 h under argon. The reactant was extracted with ethyl acetate and brine. The resulting solid was purified by column chromatography (solvent system: V(CH<sub>2</sub>Cl<sub>2</sub>)/V(petroleum ether) = 1/1) to obtain solid **2**. <sup>1</sup>H NMR for **2** (400 MHz, CDCl<sub>3</sub>):  $\delta$  = 8.74 (d, 2H), 7.61 (d, 2H), 7.26 (d, 2H), 4.79 (s, 4H), 1.42 (s, 18H). MALDI-TOF:528.6

Compound **(3)**<sup>49</sup>: To a solution of *t*-Boc TDPP (**2**, 2.50 g, 4.73 mmol) in anhydrous DMF (30 mL) was added *N*-bromosuccinimide in portion (0.926 g, 5.20 mmol). The reaction mixture was stirred at room temperature in dark under argon. After stirring for 24 h, the resulting mixture was poured into methanol and the resulting precipitate was collected by filtration. Compound **3** were separated by column chromatography (solvent system: V(CH<sub>2</sub>Cl<sub>2</sub>)/V(petroleum ether) = 2/1). <sup>1</sup>H NMR for **3** (400 MHz, CDCl<sub>3</sub>):  $\delta$  = 8.28 (d, 2H), 7.16 (d, 2H), 4.62 (s, 4H), 1.42 (s, 18H). MALDI-TOF:686.4.

Compound **(4)**<sup>50</sup>: A 30 ml anhydrous toluene solution of compound **3** (206 mg, 0.30 mmol) and Trimethyl stannane compounds (248.4 mg, 0.75 mmol) in a molar ratio of 1: 2.5 were put into a flask under argon. After 10 min argon-blowing of the solution, catalyst of Pd(PPh<sub>3</sub>)<sub>4</sub> (0.1 eq) was added to the reaction and the reactant was heated to reflux at 120 °C for 24 h. Then the reactant was cooled to room temperature. Subsequently, the solvent was removed under vacuum and the reactant was purified by silica gel chromatography (solvent system: V(CH<sub>2</sub>Cl<sub>2</sub>)/V(petroleum ether) = 2/1). <sup>1</sup>H NMR for **4** (400 MHz, CDCl<sub>3</sub>):  $\delta$  = 8.01 (d, 4H), 7.61 (d, 4H), 7.02 (d, 4H), 6.95 (d, 4H), 4.22 (s, 4H), 2.88 (m, 4H), 1.92 (m, 4H), 1.69 (m, 4H), 1.42 (s, 18H), 1.26-1.38 (m, 6H). MALDI-TOF:861.2.

Following chromatographic purification, the tert-butyl groups were removed in  $\text{CH}_2\text{Cl}_2$ /trifluoroacetic acid (TFA) mixed solvent<sup>51</sup>. In a typical reaction, 0.03 g of the protected TDPP was dissolved in 10 mL of  $\text{CH}_2\text{Cl}_2$  and TFA (V: V = 5:1) mixture solvent. The solution was stirred at room temperature for about 1 h. The progress of the reaction was followed by analytical TLC. Once the removal of all tert-butyl groups was clearly indicated by TLC results, the solvents were removed under reduced pressure followed by drying in vacuo. Dye molecule 3 was obtained. <sup>1</sup>H NMR for TDPP (400 MHz,  $\text{CDCl}_3$ ):  $\delta$  = 10.04 (d, 2H), 7.94 (d, 2H), 7.88 (d, 2H), 7.60 (d, 2H), 4.21 (s, 4H). MALDI-TOF: 416.4. Analogous procedures were repeated for TTDPP. <sup>1</sup>H NMR for TTDPP (400 MHz,  $\text{CDCl}_3$ ):  $\delta$  = 10.02 (d, 2H), 8.01 (d, 4H), 7.61 (d, 4H), 7.02 (d, 4H), 6.95 (d, 4H), 4.22 (s, 4H), 2.88 (m, 4H), 1.92 (m, 4H), 1.69 (m, 4H), 1.26-1.38 (m, 6H). MALDI-TOF: 748.9.

### Preparation of ZnO nanorods

ZnO nanorods were prepared through treatment of a methanolic solution of zinc(II) diacetate with KOH as a base, following an experiment process similar to that reported in literatures.<sup>51, 52</sup> All materials were purchased from Sigma-Aldrich and used as received.

### Fabrication of hybrid materials

2 mg dry ZnO NRs was dissolved in 2 mL THF solution of TDPP ( $2.79 \times 10^{-5}$  M) and TTDPP ( $1.64 \times 10^{-5}$  M) in ultrasonic bath for 30 min for assembly of ZnO NRs. The mixture was centrifugated and washed by THF for three times. The solution of TDPP/ZnO and TTDPP/ZnO was obtained by re-dispersed the remains into 2 mL THF. By taking an average surface per ZnO nanorod ( $10 \times 100$  nm) of  $3140 \text{ nm}^2$  and an average surface per TDPP and TTDPP molecule of 1.26 and  $2.41 \text{ nm}^2$  respectively, this corresponds to an average surface coverage of 45% and 51%, respectively.

### Conclusions

In summary, two organic compounds of TDPP and TTDPP were successfully grafted on the surface of n-type inorganic semiconductor ZnO nanorods using carboxylic acid end group as functional ligand. Strong quenching of the fluorescence of TDPP and TTDPP moiety were observed after the grafting of TDPP and TTDPP on the surface of ZnO nanorods, suggesting efficient interface charge transfer process from TDPP or TTDPP chromophore to ZnO nanorods. High performance visible-light photodetector based on TTDPP/ZnO has been fabricated with high responsivity of 16.9 A/W and an on/off ratio as high as  $\sim 10^4$ . The excellent visible-light photoresponse of the hybrid device can be attributed to the broadband absorption after the anchoring of TTDPP compound on the surface of ZnO nanorods, the efficient cascade electron transfer process and the excellent capability of ZnO nanorod to provide direct and stable pathways for the transport of photogenerated electrons toward the collection electrode. The high visible-light response of the as-prepared hybrid device TTDPP/ZnO makes it a promising candidate for applications in photo-to-electrical energy conversion.

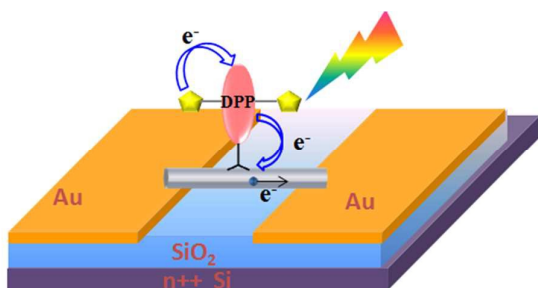
### Acknowledgements

This work was supported by the National Natural Science Foundation of China (Nos. 21403130, 20373077, 20925309, 21190034, 21221002, 21373239), Natural Science Foundation of Shandong Province (ZR2014BQ028), Chinese Academy of Sciences, and the National Basic Research Program of China (973) 2011CB808402.

### References

- S. Zhang, C. I. Pelligra, G. Keskar, J. Jiang, P. W. Majewski, A. D. Taylor, S. Ismail-Beigi, L. D. Pfefferle and C. O. Osuji, *Adv Mater*, 2012, **24**, 82-87.
- J. J. Wang, Y. Q. Wang, F. F. Cao, Y. G. Guo and L. J. Wan, *J Am Chem Soc*, 2010, **132**, 12218-12221.
- S. Yang, X. Cui, J. Gong and Y. Deng, *Chem Commun*, 2013, **49**, 4676-4678.
- Y. Guo, C. Liu, H. Tanaka and E. Nakamura, *The Journal of Physical Chemistry Letters*, 2015, **6**, 535-539.
- A. Ghadirzadeh, L. Passoni, G. Grancini, G. Terraneo, A. Li Bassi, A. Petrozza and F. Di Fonzo, *ACS Applied Materials & Interfaces*, 2015, **7**, 7451-7455.
- D. Shao, J. Gao, P. Chow, H. Sun, G. Xin, P. Sharma, J. Lian, N. A. Koratkar and S. Sawyer, *Nano Lett*, 2015, DOI: 10.1021/acs.nanolett.5b00380.
- D. Shao, M. Yu, H. Sun, G. Xin, J. Lian and S. Sawyer, *ACS Applied Materials & Interfaces*, 2014, **6**, 14690-14694.
- S. Roland, S. Neubert, S. Albrecht, B. Stannowski, M. Seger, A. Facchetti, R. Schlatmann, B. Rech and D. Neher, *Adv Mater*, 2015, **27**, 1262-1267.
- S. Ghosh, A. H. Khan and S. Acharya, *The Journal of Physical Chemistry C*, 2012, **116**, 6022-6030.
- Z. Yin and Q. Zheng, *Advanced Energy Materials*, 2012, **2**, 179-218.
- D. V. Talapin, J. S. Lee, M. V. Kovalenko and E. V. Shevchenko, *Chem Rev*, 2010, **110**, 389.
- T. M. Clarke and J. R. Durrant, *Chem Rev*, 2010, **110**, 6736-6767.
- K. E. Linton, M. A. Fox, L.-O. Pålsson and M. R. Bryce, *Chemistry – A European Journal*, 2015, **21**, 3997-4007.
- Y.-Z. Long, M.-M. Li, C. Gu, M. Wan, J.-L. Duvail, Z. Liu and Z. Fan, *Prog Polym Sci*, 2011, **36**, 1415-1442.
- A. L. Briseno, T. W. Holcombe, A. I. Boukai, E. C. Garnett, S. W. Shelton, J. J. M. Fréchet and P. Yang, *Nano Lett*, 2010, **10**, 334-340.
- B. Mallampati, S. V. Nair, H. E. Ruda and U. Philipose, *J Nanopart Res*, 2015, **17**, 1-10.
- Z. Jin and J. Wang, *Journal of Materials Chemistry C*, 2014, **2**, 1966-1970.
- H. Yan, Z. Yu, K. Lu, Y. Zhang and Z. Wei, *Small*, 2011, **7**, 3472-3478.
- B. J. Richardson, X. Wang, A. Almutairi and Q. Yu, *Journal of Materials Chemistry A*, 2015, **3**, 5563-5571.

20. D. Bi, F. Wu, W. Yue, Y. Guo, W. Shen, R. Peng, H. Wu, X. Wang and M. Wang, *The Journal of Physical Chemistry C*, 2010, **114**, 13846-13852.
21. O. Pachoumi, A. A. Bakulin, A. Sadhanala, H. Sirringhaus, R. H. Friend and Y. Vaynzof, *The Journal of Physical Chemistry C*, 2014, **118**, 18945-18950.
22. S. Obuchovsky, I. Deckman, M. Moshonov, T. Segal Peretz, G. Ankonina, T. J. Savenije and G. L. Frey, *Journal of Materials Chemistry C*, 2014, **2**, 8903-8910.
23. K. P. Musselman, S. Albert-Seifried, R. L. Z. Hoyer, A. Sadhanala, D. Muñoz-Rojas, J. L. MacManus-Driscoll and R. H. Friend, *Adv Funct Mater*, 2014, **24**, 3562-3570.
24. Y. Vaynzof, A. A. Bakulin, S. Gélinas and R. H. Friend, *Phys Rev Lett*, 2012, **108**, 246605.
25. M. Kaur and D. H. Choi, *Chemical Society Reviews*, 2015, **44**, 58-77.
26. S. Zhang, L. Ye, Q. Wang, Z. Li, X. Guo, L. Huo, H. Fan and J. Hou, *The Journal of Physical Chemistry C*, 2013, **117**, 9550-9557.
27. V. S. Gevaerts, E. M. Herzig, M. Kirkus, K. H. Hendriks, M. M. Wienk, J. Perlich, P. Müller-Buschbaum and R. A. J. Janssen, *Chem Mater*, 2013, **26**, 916-926.
28. J. Huang, C. Zhan, X. Zhang, Y. Zhao, Z. Lu, H. Jia, B. Jiang, J. Ye, S. Zhang, A. Tang, Y. Liu, Q. Pei and J. Yao, *ACS Applied Materials & Interfaces*, 2013, **5**, 2033-2039.
29. H. Li, F. Liu, X. Wang, C. Gu, P. Wang and H. Fu, *Macromolecules*, 2013, **46**, 9211-9219.
30. Y. S. Kwon, J. Lim, H.-J. Yun, Y.-H. Kim and T. Park, *Energy & Environmental Science*, 2014, **7**, 1454-1460.
31. Z. Huang, E. C. Fregoso, S. Dimitrov, P. S. Tuladhar, Y. W. Soon, H. Bronstein, I. Meager, W. Zhang, I. McCulloch and J. R. Durrant, *Journal of Materials Chemistry A*, 2014, **2**, 19282-19289.
32. W. Li, W. S. C. Roelofs, M. Turbiez, M. M. Wienk and R. A. J. Janssen, *Adv Mater*, 2014, **26**, 3304-3309.
33. E. Zhou, S. Yamakawa, K. Tajima, C. Yang and K. Hashimoto, *Chem Mater*, 2009, **21**, 4055-4061.
34. W. Li, A. Furlan, W. S. C. Roelofs, K. H. Hendriks, G. W. P. van Pruissen, M. M. Wienk and R. A. J. Janssen, *Chem Commun*, 2014, **50**, 679-681.
35. C. J. Mueller, C. R. Singh, M. Fried, S. Huettner and M. Thelakkat, *Adv Funct Mater*, 2015, **25**, 2725-2736.
36. K. H. Hendriks, W. Li, G. H. L. Heintges, G. W. P. van Pruissen, M. M. Wienk and R. A. J. Janssen, *J Am Chem Soc*, 2014, **136**, 11128-11133.
37. R. S. Ashraf, I. Meager, M. Nikolka, M. Kirkus, M. Planells, B. C. Schroeder, S. Holliday, M. Hurhangee, C. B. Nielsen, H. Sirringhaus and I. McCulloch, *J Am Chem Soc*, 2015, **137**, 1314-1321.
38. H. Liu, H. Jia, L. Wang, Y. Wu, C. Zhan, H. Fu and J. Yao, *Phys Chem Chem Phys*, 2012, **14**, 14262-14269.
39. Y. Wu, Y. Li, H. Li, Q. Shi, H. Fu and J. Yao, *Chem Commun*, 2009, DOI: 10.1039/b914103k, 6955-6957.
40. M. Sofos, J. Goldberger, D. A. Stone, J. E. Allen, Q. Ma, D. J. Herman, W.-W. Tsai, L. J. Lauhon and S. I. Stupp, *Nat Mater*, 2009, **8**, 68-75.
41. Y. Jin, J. Wang, B. Sun, J. C. Blakesley and N. C. Greenham, *Nano Lett*, 2008, **8**, 1649-1653.
42. C. Soci, A. Zhang, B. Xiang, S. A. Dayeh, D. P. R. Aplin, J. Park, X. Y. Bao, Y. H. Lo and D. Wang, *Nano Lett*, 2007, **7**, 1003-1009.
43. G. Konstantatos and E. H. Sargent, *Nat Nano*, 2010, **5**, 391-400.
44. H. Kind, H. Yan, B. Messer, M. Law and P. Yang, *Adv Mater*, 2002, **14**, 158-160.
45. J.-J. Wang, J.-S. Hu, Y.-G. Guo and L.-J. Wan, *J Mater Chem*, 2011, **21**, 17582-17589.
46. Y. Jiang, W. J. Zhang, J. S. Jie, X. M. Meng, X. Fan and S. T. Lee, *Adv Funct Mater*, 2007, **17**, 1795-1800.
47. C. Pacholski, A. Kornowski and H. Weller, *Angew Chem Int Ed*, 2002, **41**, 1188-1191.
48. Y. Suna, J.-i. Nishida, Y. Fujisaki and Y. Yamashita, *Organic Letters*, 2012, **14**, 3356-3359.
49. A. D. Hendsbee, J.-P. Sun, L. R. Rutledge, I. G. Hill and G. C. Welch, *Journal of Materials Chemistry A*, 2014, **2**, 4198-4207.
50. P. Sonar, T. R. B. Foong and A. Dodabalapur, *Phys Chem Chem Phys*, 2014, **16**, 4275-4283.
51. F. Yukruk, A. L. Dogan, H. Canpinar, D. Guc and E. U. Akkaya, *Organic Letters*, 2005, **7**, 2885-2887.
52. B. Sun and H. Sirringhaus, *Nano Lett*, 2005, **5**, 2408-2413.



High photoresponse covering the UV-vis region was realized in TTDPP/ZnO hybrid system, which is attributed to efficient cascade electron transfer process.